Ferroelectric properties of $[4\text{-}NH_2C_5H_4NH][SbCl_4]$

R. Jakubas, Z. Ciunik, and G. Bator
Faculty of Chemistry, University of Wrocław, 50-383 Wrocław, Joliot Curie 14, Poland
(Received 20 May 2002; published 13 January 2003)

A ferroelectric crystal $[4\text{-}NH_2C_5H_4NH][SbCl_4]$ has been synthesized. The x-ray diffraction studies indicate that it is made of polyanionic chains of $(SbCl_4^-)_n$ forming a tunnel-like structure and the 4-aminopyridinium cations connected via weak hydrogen bonds to the chlorine atoms. The x-ray and differential scanning calorimetry studies show that the crystal undergoes a complex sequence of phase transitions: $P2_1/c \overset{240/245\ K}{\longleftrightarrow} (Cc) \overset{248.5/250\ K}{\longleftrightarrow} Cc \overset{270.5/271\ K}{\longleftrightarrow} C2/c \overset{304/304\ K}{\longleftrightarrow} C2/c$. The pyroelectric measurements reveal that $[4\text{-}NH_2C_5H_4NH][SbCl_4]$ becomes ferroelectric below 270.5 K with the spontaneous polarization of the order of 3.5 mC/m^2 measured along the [102] direction. The dielectric results confirm the order-disorder nature of the paraelectric-ferroelectric phase transition. The dynamics of the 4-aminopyridinium cations plays an essential role in the ferroelectric phase transition mechanism.

DOI: 10.1103/PhysRevB.67.024103 PACS number(s): 77.80.Bh, 77.70.+a, 61.10.−i

I. INTRODUCTION

Recently, the alkylammonium halogenoantimonates(III) and bismuthates(III) of the general formula $R_aM_bX_{3b+a}$ (where *R* denotes organic cations, *M* denotes Sb, Bi, and *X* denotes Cl, Br, I) were intensively investigated.[1–3] It was found that numerous compounds of this family exhibited multiple structural phase transitions. We were particularly interested in salts with the $R_3M_2X_9$ or $R_5M_2X_{11}$ compositions since they frequently demonstrated ferroelectric properties. The crystal structure of the $R_3M_2X_9$ subclass was characterized by three types of anionic form: (1) zigzag double chains,[4] (2) two-dimensional layers of the MX_6 octahedra,[5] and (3) discrete $M_2X_9^{3-}$ units.[6] It was shown that polar properties appear only for the salts built up of the layer anionic sublattice and small-sized organic cations, such as $CH_3NH_3^+$, $(CH_3)_2NH_2^+$, and $(CH_3)_3NH^+$.[7–10] The second subclass mentioned above, $R_5M_2X_{11}$, was characterized exclusively by discrete $M_2X_{11}^{5-}$ units. Up to now there are known only three salts crystallizing with this composition: $(CH_3NH_3)_5Bi_2Br_{11}$,[11] $(CH_3NH_3)_5Bi_2Cl_{11}$,[12] and $(C_5H_5NH)_5Bi_2Br_{11}$.[13] All of them appeared to have ferroelectric properties. Their paraelectric-ferroelectric phase transitions were classified as an ''order-disorder'' type. The origin of the ferroelectricity of both subclasses was attributed to a dynamics of dipolar organic cations.

In searching for different ferroelectrics from the halogenoantimonate(III) and bismuthate(III) family we have synthesized 4-aminopyridinium tetrachloroantimonate(III), $[4\text{-}NH_2C_5H_4NH][SbCl_4]$. It should be emphasized that $[4\text{-}NH_2C_5H_4NH][SbCl_4]$ appeared to be the first known example of a molecular-ionic ferroelectric containing in the crystal structure substituted pyridinium cation [e.g., 4-aminopyridinium (4AP)].

In this paper we present results of x-ray, differential scanning calorimetry, dielectric, and pyroelectric studies on the ferroelectric $[4\text{-}NH_2C_5H_4NH][SbCl_4]$ crystal. The mechanism of the paraelectric-ferroelectric phase transition is discussed.

II. EXPERIMENT

Single crystals of $[4\text{-}NH_2C_5H_4NH][SbCl_4]$ were grown by a slow evaporation method at room temperature from an aqueous solution containing $4\text{-}NH_2C_5H_4NHCl$ and Sb_2O_3 in an equimolar ratio and excess of HCl. Differential scanning calorimetry (DSC) was recorded using a Perkin Elmer DSC-7 calorimeter in the temperature range 100–400 K with the scanning rates from 5 to 20 K/min. The complex electric permittivity $\varepsilon^* = \varepsilon' - i\varepsilon''$ was measured by a HP 4284A Precision *LCR* meter in the frequency range between 100 kHz and 1 MHz in the temperature range from 230 to 300 K. The dimensions of the sample were of the order of $5 \times 3 \times 1\ mm^3$. The overall error was less than 5% and 10% for the real and imaginary part of the complex electric permittivity, respectively.

The spontaneous polarization was measured between 230 and 300 K by a charge integration technique using a Keithley 617 programmable electrometer. The temperature was stabilized by an Instec STC200 temperature controller.

A colorless monoclinic-shaped crystal of dimensions $0.11 \times 0.15 \times 0.15$ mm was used for data collection for x-ray diffraction. All measurements of the crystal were performed using an Oxford Cryosystem device on a Kuma KM4 κ-axis diffractometer with graphite-monochromated Mo $K\alpha$ radiation and a charger coupled device (CCD) detector. Accurate cell parameters were determined and refined by a least-squares fit of angular data of 1714 of the strongest reflections at 278 K, 1919 reflections at 258 K, 1784 reflections at 243 K, 3605 reflections at 100 K, and finally 1655 reflections at 308 K. Space groups were determined from all reflections collected at fixed temperatures. Data collections, integration, scaling of the reflections, and absorption were made using the CrysAlis suite of programs.[14] The structures of crystals were solved using the heavy-atom method with the SHELXS97 program[15] and refined by the full-matrix least-squares method on all F^2 data using the SHELXL97 programs.[16] At 278 K the parameters of the Sb, Cl, and N atoms from amino groups were refined with anisotropic displacement parameters, whereas the nonhydrogen atoms from the aromatic rings were refined isotropically with idealized geometry. At

 ©2003 The American Physical Society

TABLE I. Structure determination and refinement results for $[4\text{-}NH_2C_5H_4NH][SbCl_4]$.

Structure at Phase	278 K II	258 K III	100 K V
Space group:	$C2/c$ (No. 15)	Cc (No. 9)	$P2_1/c$ (No. 14)
a (Å)	13.356(2)	13.322(2)	7.956(1)
b (Å)	12.722(2)	38.001(5)	12.437(1)
c (Å)	7.867(1)	7.888(1)	10.900(1)
β (deg)	123.82(1)	123.87(1)	93.28(1)
V (Å^3)	1110.6(3)	3315.7(8)	1076.8(1)
Z	4	12	4
θ_{max}	28.39	28.43	28.40
Reflections collected	3684	11375	7211
Independent reflections	1278	4972	2492
$S(F^2)$	1.100	0.950	1.070
$R_1(F)$	0.0472	0.0428	0.0251
$wR_2(F^2)$	0.1194	0.0814	0.0549

this temperature the hydrogen atoms were not included for these calculations. At 258 K all nonhydrogen atoms were refined with anisotropic displacement parameters and H atoms were fixed. At 100 K all nonhydrogen atoms were refined with anisotropic and H atoms with isotropic displacement parameters.

Crystallographic data for the structures reported in this paper (excluding structure factors) have been deposited with the Cambridge Crystallographic Data Center.[17]

III. RESULTS

Table I summarizes the results for structures at 278, 258, and 100 K. The crystallographic data obtained at several temperatures between room temperature and 100 K show an existence of three reversible phase transitions. At all transitions the structure changes from one monoclinic to another monoclinic symmetry. Moreover, at 278 K a coexistence of two lattices with different monoclinic space groups are usually observed for virgin crystals (80% of the space group $C2/c$, 20% of noncentrosymmetric lattice with the b parameter tripled and the space group Cc). At 258 K the space group Cc is exclusively observed and the lattice parameters are close to those for the noncentrosymmetric ones observed at 278 K. At 243 K the space group Cc is indicated only by 83% of reflections. Determination of Miller indices for remaining reflections was unsuccessful. At 100 K the space group $P2_1/c$ is determined by all of the reflections as a unique-space group. After subsequent heating of the crystal to 278 K, and then to 308 K, all the reflections indicate parameters of the centrosymmetric lattice with the space group $C2/c$. The projection of the crystal structure of $[4\text{-}NH_2C_5H_4NH][SbCl_4]$ in the c direction at 258 K is shown in Fig. 1.

A detailed analysis of the x-ray results shows that all the phase transitions in $[4\text{-}NH_2C_5H_4NH][SbCl_4]$ are not accompanied by any significant deformation of the anionic sublattice. This means that the hydrogen-bond system is not significantly reorganized. The N-H$\cdots$Cl hydrogen bonds being of the order of 3.24–3.28 Å are classified as weak. Despite the small strength of the hydrogen bonds the cations seem to be strongly stabilized in the lattice. We should consider thus two additional factors influencing the dynamics of the cations. First, the cations are stabilized by hydrogen bonding simultaneously to two N atoms being in the para position in the ring. Second, a cation is characterized by a quite large inertia moment for the C_6' motion, i.e., for rotation about the pseudohexagonal axis of the pyridinium ring. This causes a subtle balance with the dipole-dipole interactions, which affects ordering of dipolar groups in the lattice.

The DSC curves of the $[4\text{-}NH_2C_5H_4NH][SbCl_4]$ crystals for cooling and heating runs are shown in Fig. 2. Calorimetric measurements indicate a complex sequence of phase transitions in $[4\text{-}NH_2C_5H_4NH][SbCl_4]$: at 304 K a phase transition of second order, at 270.5/271 K (cooling/heating) close to first order, at 248.5/250.5 K and 240/245 K both phase transitions of clearly first-order type. The transition entropy value (ΔS) is equal to 3.5 J mol^{-1} K^{-1} for the 240 K phase transition, whereas for the 248.5 and 270.5 K transitions it is distinctly below 1 J mol^{-1} K^{-1}. When the ΔS value is considered, only the phase transition at 240 K may be classified as an ''order-disorder'' type.

From the x-ray examination at 258 K the space group Cc is found, which implies that the polar axis lies in the a-c

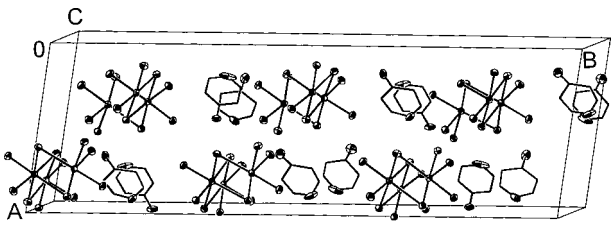

FIG. 1. Unit cell of $[4\text{-}NH_2C_5H_4NH][SbCl_4]$ viewed along the c axis in the ferroelectric phase Cc. The thermal ellipsoids are drawn at 50% probability for the chlorine and antimony atoms of the anionic units as well as for the nitrogen atoms of the organic cations.

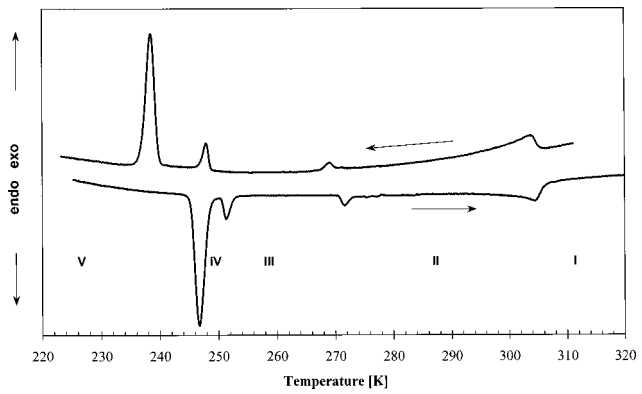

FIG. 2. DSC curves for the $[4\text{-}NH_2C_5H_4NH][SbCl_4]$ crystals at the cooling and heating runs between 220 and 320 K (10 K min^{-1}, $m=9.34$ mg).

plane. The complex electric permittivity, $\varepsilon^*=\varepsilon'-i\varepsilon''$, measured along the *a*,*b*,*c* axes and [102] direction of the monoclinic system for $[4\text{-}NH_2C_5H_4NH][SbCl_4]$ is shown in Fig. 3. Along the [102] directions, ε'_{max} reaches a value of about 700 units at $T_{c2}=270.5$ K. Since the imaginary part, $\varepsilon''_{[102]}$, at 100 Hz is relatively small ($\tan\delta<0.1$) for the temperature range $T>T_{c2}+0.2$ K, $\varepsilon'_{[102]}$ measured at this frequency may

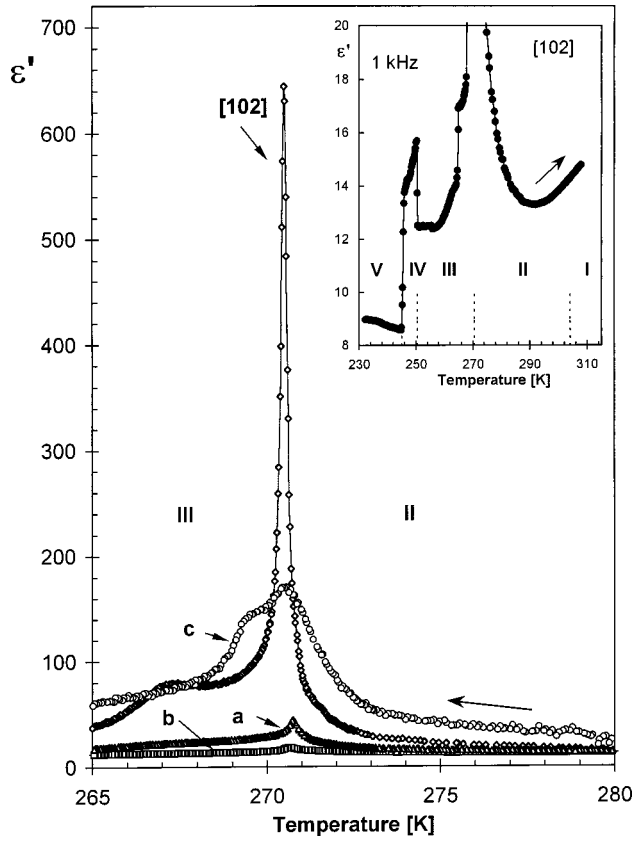

FIG. 3. Temperature dependence of the electric permittivity ε' along the [102] direction and along the *a*, *b*, and *c* axes at 100 Hz for $[4\text{-}NH_2C_5H_4NH][SbCl_4]$ in the vicinity of paraelectric-ferroelectric phase transition (II→III). The inset shows ε' vs temperature covering all the phases during heating (at 1 kHz).

be regarded as a static electric permittivity (ε_0). The broad peak in the $\varepsilon'_{[102]}$ value at about 268 K (in the ferroelectric phase) may be caused by the domain-wall motion since the position of this peak changes with increase of frequency of the applied ac electric field. The measurements of the electric permittivity performed along the *a*, *b*, and *c* directions show smaller ε' and ε'' values close to T_c, which means that only the projection of the resultant dipole moments of the unit cell for these directions is seen.

The measurements of the ε_0 value performed along the *a*, *b* and *c* axes as well as along directions perpendicular to the *a* and *c* axes (except for the [102] direction) allowed us to determine the components of the electric permittivity tensor. The measurements were carried out for samples cut from the same single crystal. The corresponding ε values at T_c are as follows: 44, 18, 170, 326, and 179 along the *a*, *b*, and *c* axes and directions perpendicular to the *a* and *c* axes, respectively. The calculated tensor is presented below:

$$\begin{bmatrix} 340 & 0 & 0 \\ 0 & 18 & 0 \\ 0 & 0 & 63 \end{bmatrix}$$

with the ε_{max} orientation about 78° from the *a* axis and 45.8° from the *c* axis. We should add that this direction inclined towards the *c* axis from the [102] direction by 7° in the *a*-*c* plane. It should be noted that the obtained $\varepsilon_{max}=340$ is remarkably lower than that presented in Fig. 3. This is a result of the worse quality of the single crystal used for the measurements of the permittivity anisotropy. The more accurate measurements of the permittivity anisotropy in the $[4\text{-}NH_2C_5H_4NH][SbCl_4]$ crystal is planned in the near future. It is also interesting that we observe an enhanced ε value along the *c* axis in the wide temperature range except for that in the close vicinity of T_c. This may be explained by the fact that the polyanionic chains extend along the *c* axis, and a larger contribution of the anionic sublattice to the crystal polarizability may be expected.

The inset in Fig. 3 shows $\varepsilon'_{[102]}$ versus temperature between 230 and 310 K during heating. The phase transitions at 248.5 and 240 K are clearly seen as a sharp jump in the ε' value. Since the IV→V phase transition is accompanied by a partial cracking of the single crystal, the $\varepsilon'_{[102]}$ versus temperature scan only during heating is shown.

The $1/\varepsilon'_{[102]}$ versus temperature representation (see Fig. 4) usually reveals both the order of the phase transition and the Curie-Weiss constants according to the well-known formula for ferroelectric crystals: $\varepsilon_0=C_{+/-}/(T-T_c)$, where C_+ and C_- are constants for the paraelectric and ferroelectric phases, respectively, and T_c is the phase transition temperature ($C_+/C_-=4$ and 2 for the first- and second-order phase transition, respectively). In this case, however, in the paraelectric phase the Curie-Weiss law is not well obeyed. The Curie-Weiss constant increases from $C_+=48$ to 97 K in the temperature range 271–273 K and is even larger at higher temperature. It should be noticed that the electric permittivity was measured in the dispersion frequency region either in the paraelectric or ferroelectric phase (100 Hz–1

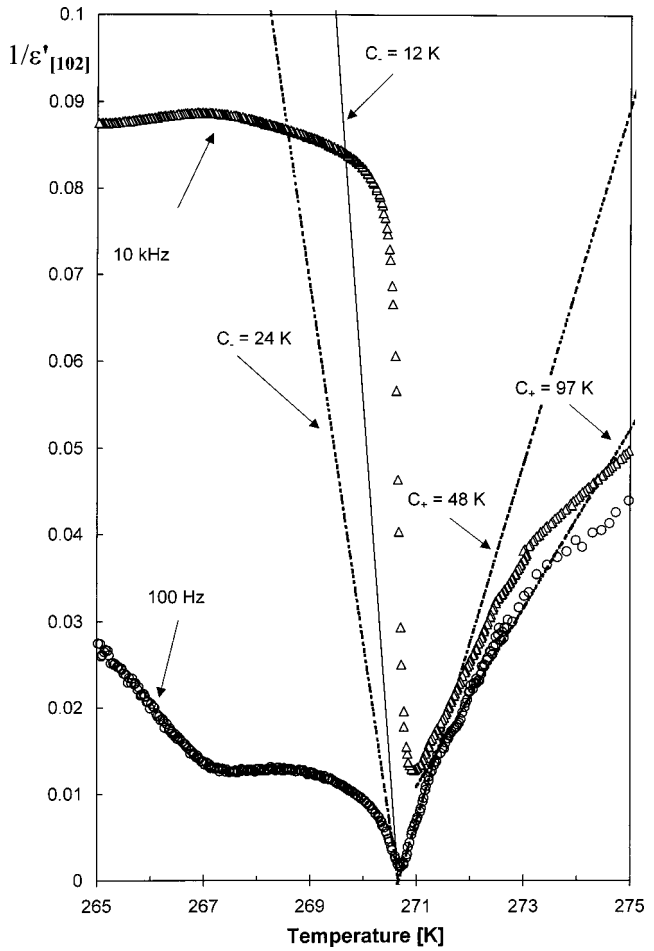

FIG. 4. Reciprocal ε' as a function of temperature measured at 100 Hz (○) and 10 kHz (△). The broken line below 270.5 K shows the theoretical results assuming the pure second-order transition ($C_- = 24$ K) and the solid line the first-order phase transition ($C_- = 12$ K). The two broken lines above T_c correspond to two temperature regions where the Curie-Weiss law parameters were estimated.

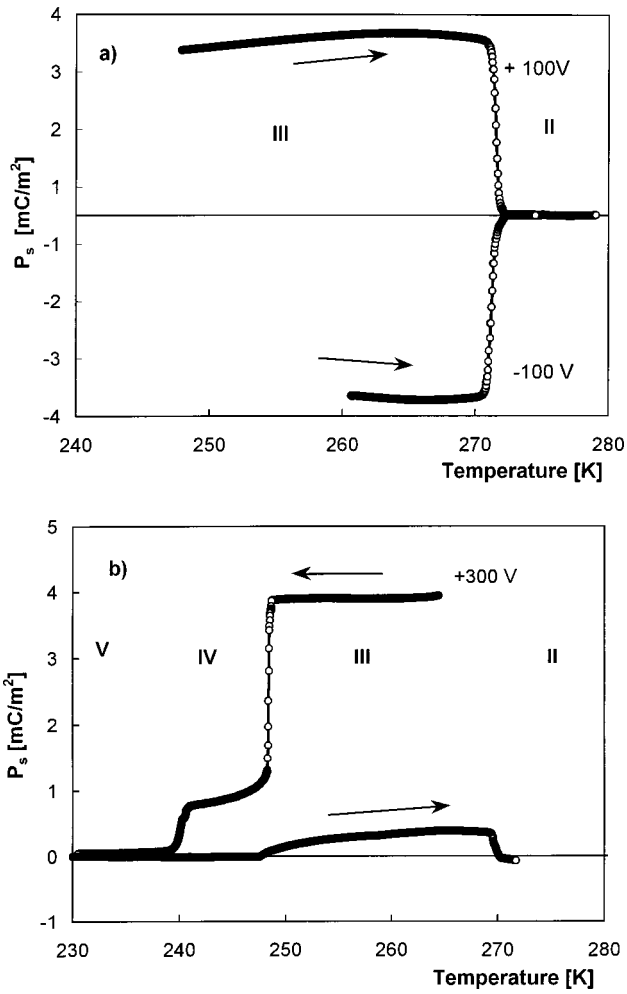

FIG. 5. (a) Spontaneous polarization P_s as a function of temperature obtained on warming by pyroelectric measurements after poling the crystal (± 1 kV cm^{-1}). (b) The temperature dependence of P_s on cooling from $T = 265$ K below the IV→V phase transition and on heating to phase II without any poling.

MHz). It is thus impossible to estimate the value C_- since we observe a participation of the domain-wall motion in ε' at the applied frequencies of the measuring electric field.

Preliminary dielectric dispersion studies show that fundamental ferroelectric dispersion in $[4\text{-}NH_2C_5H_4NH][SbCl_4]$ over the paraelectric phase appears in the kiloherz frequency range. These results confirm the order-disorder nature of the ferroelectric transition.

The pyroelectric current was then measured after poling the crystal while cooling from room temperature down to ~265 K (to keep the crystal within phase III). The dc electric field was equal to +1 kV/cm. The pyroelectric current I_{pyro} was then measured during the temperature increase. Furthermore, the crystal was cooled when poling by the dc electric field of the negative value of −1 kV/cm to the temperature 260 K. The same procedure was used in order to obtain the change of P_s at T_{c2} during heating.

The spontaneous polarization (P_s) as a function of temperature is shown in Fig. 5(a). It is clearly seen that P_s is reversed by the dc electric field and that it is equal to about 3.5×10^{-3} C/m^2 at 265 K. This is proof that $[4\text{-}NH_2C_5H_4NH][SbCl_4]$ becomes ferroelectric below the 270.5 K phase transition point.

From the x-ray results we might conclude that below $T_{c4} = 240$ K the crystal becomes nonpolar again. To check this supposition, the measurements of the pyroelectric current in the temperature range 230–300 K were undertaken. First, the crystal was cooled from 280 to 265 K using an external electric field as large as 3 kV/cm. Then the pyroelectric current was measured during cooling to 230 K. The result of the integration of the pyroelectric current, i.e., the polarization versus temperature, is shown in Fig. 5(b). At $T_{c3} = 248.5$ K the stepwise drop of P_s is observed to a value of about 1×10^{-3} C/m^2 and then at $T_{c4} = 240$ K, the spontaneous polarization completely disappears. It means that the crystal undergoes a phase transition to a nonpolar phase. When the crystal is then heated from 230 K, at the V→IV phase transition point, P_s appears again but a drastic reduction of its value, in comparison to that obtained during cool-

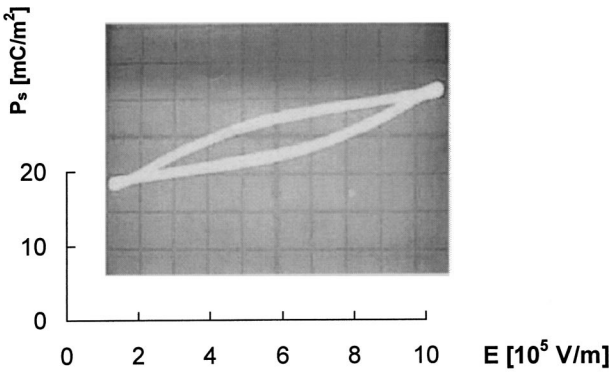

FIG. 6. Dielectric hysteresis loop observed along the [102] direction at 270 K.

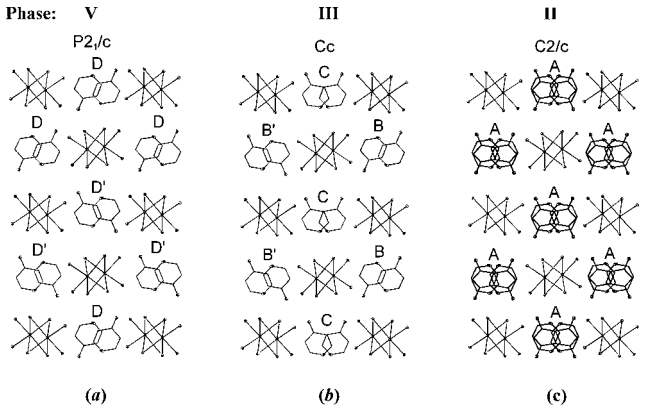

FIG. 7. Schematic view of molecular packing diagrams in $[4\text{-}NH_2C_5H_4NH][SbCl_4]$ (a) in the low-temperature phase at 100 K, (b) in ferroelectric phase at 258 K, and (c) in the high-temperature paraelectric phase at 278 K.

ing, is found. It may be a result of the fact that the we deal with a multidomain state in the sample. At $T_{c2}=271$ K (while heating) P_s drops again to zero, which is obviously expected. The observed temperature dependence of P_s is in perfect accordance with the x-ray results.

The P_s versus temperature curve (see Fig. 5) is characteristic of ferroelectrics with a first-order transition. In addition, because of the visible temperature hysteresis ($\Delta T \approx 0.5$ K) and the heat effect in the DSC measurement, this material may be treated as a ferroelectric with the phase transition close to first-order type. For such a type of ferroelectrics one can use the following formula.[18]

$$\Delta S = \tfrac{1}{2}\beta P_{sc}^2,$$

where ΔS is the entropy change, P_{sc} is a value of the spontaneous polarization close to T_c (in our case $P_{sc} \approx 2$ mC/m^2 at $T=T_c-0.5$), and $\beta = 1/\varepsilon_0 C$ with C the average Curie constant obtained from the Curie-Weiss law in the paraelectric phase ($C_+ = 70$ K). The computed value ΔS is equal to 0.54 J/mol K. The agreement is not very good with the experimental value of $\Delta S \approx 0.2 \pm 0.05$ J/mol K. But we should remember that ΔS obtained from DSC measurements is burdened by a large error, especially for quite weak first-order transitions. The most important conclusion is that the expected ΔS value for the paraelectric-ferroelectric phase transition should be relatively small, which is really observed in our experiment.

The existence of the ferroelectric phase in $[4\text{-}NH_2C_5H_4NH][SbCl_4]$ was also confirmed by an examination of the *D-E* hysteresis loop below $T_{c2}=270.5/271$ K (the crystal was cooled down and warmed up repeatedly through T_{c2}). A clear ferroelectric hysteresis loop could be observed at 3 kV/cm (at 50 Hz) along the [102] direction (see Fig. 6).

IV. DISCUSSION

Structures at all fixed temperatures show a simple, very similar molecular packing: parallel anionic chains of $(SbCl_4^-)_n$ surrounded by the 4AP cations. Figure 7 illustrates the most important details of molecular packing in the three phases. All diagrams are oriented along the axes of the anionic chains. Near room temperature the anionic chains are parallel to the [001] direction and the cations located near the twofold axes are disordered in the ratio 1:1 [case A in Fig. 7(c)]. Their rings are oriented parallel to the plane (201) of the crystal. At 258 K and partly at 243 K [see Fig. 7(b)] the 4AP cations have three different symmetry-independent orientations. In case *C* the long axes of the cations defined by a N-NH_2 vector of molecule form a small angle with the [102] direction. In both remaining cases, *B* and *B′*, they have two different antiparallel orientations so they do not contribute to the P_s value. In this phase the pyridinium rings are parallel to the same plane as at the room temperature. The spontaneous polarization vector is oriented along the [102] direction of the crystal. At 100 K [Fig. 7(a)] the anionic chains are parallel to the [100] direction of the actual lattice, and long axes of cations have antiparallel, symmetry-dependent orientations, *D* and *D′*, so that there is no net polarization. The pyridinium rings are parallel to the (101) plane of the crystal. This plane corresponds to the (201) plane in the previously described phases. The nature of the polar phase between 248.5 and 240 K is not clear. Probably most of 4AP cations try to orient antiparallel to one another.

Comparison of all packing diagrams *A*, *B*/*B′*, *C*, and *D*/*D′* shows that each 4AP cation in the crystal can have two different orientations of the long molecular axis. Reorientation of the cations in the crystal is possible by rotation of about 135° around the axis perpendicular to the aromatic ring only. It should be emphasized that the relationship among all phases as well as the crystal lattices and crystallographic symmetries, which are observed in the investigated crystal, is simply related to the orientations of the cations.

We should emphasize that paraelectric-ferroelectric phase transition is accompanied by a tripling of the unit cell along the *b* axis. This implies that during this transition a number of atoms in the unit cell is changed; thus the spontaneous polarization cannot be a transition parameter. A transition of such a type is treated as an improper ferroelectric one.[19–21] The shape of the dielectric response around the paraelectric-ferroelectric phase and the relatively small value of the spontaneous polarization (3.5 mC/m^2) are also characteristic of the improper ferroelectrics.[22]

The critical slowing down of the dielectric relaxation time, which is clearly observed in preliminary dielectric dispersion studies between 100 Hz and 1 MHz,[23] confirms the dynamic behavior of an order-disorder type, such as in the case of $NaNO_2$[24] TGS,[25] and alums.[26]

Up to now the ferroelectricity in the halogenoantimonates(III) and bismuthates(III) is recognized in two classes of compounds: $R_3M_2X_9$ and $R_5M_2X_{11}$. Most ferroelectric compounds are found in the group of crystals with the former stoichiometry. It turns out that the polar properties for such crystals are strictly connected with the presence of a two-dimensional anionic layer structure. The deformation of voids inside such a layer occupied by organic cations leads to the changes in the cationic dynamics. Thus, the electric coupling of the cationic and anionic sublattices results in the long-range electric order of the ferroelectric type. A large polarizability of the $(M_2X_9{}^{3-})_n$ layers is considered as the most important factor stimulating the appearance of ferroelectricity. On the other hand, in the ferroelectric systems with $R_5Bi_2X_{11}$ composition the structural situation is completely different. Instead of the polyanionic structure, isolated bioctahedra $Bi_2X_{11}{}^{5-}$ appear. Since there is only one bridging bond in these bioctahedra, they are characterized by important flexibility. It stimulates, probably, the appearance of ferroelectricity.

In the case of $[4\text{-}NH_2C_5H_4NH][SbCl_4]$ we deal with the intermediate situation taking into account the structure of the anionic form. $[4\text{-}NH_2C_5H_4NH][SbCl_4]$ is found to be an example of a ferroelectric crystal from the halogenoantimonates(III) family characterized by one-dimensional anionic structure $(SbCl_4{}^-)_n$. The chains extend along the *c* axis, i.e., in the *a*-*c* plane containing the spontaneous polarization vector. The polarizability of the chain $(SbCl_4{}^-)_n$ is an important factor influencing the appearance of the ferroelectricity. On the other hand, it seems that the existence of the $5s^2$ electron pair of the Sb(III) atoms was not sufficiently taken into account. Our studies showed that numerous alkylammonium chloroantimonates(V) (devoid of $5s^2$ electrons) are usually characterized by quite a small electric polarizability as well as a lack of electric long-range order.[27] In conclusion, the presence of the $5s^2$ electrons of Sb atoms must play an important role in the induction of ferroelectricity in halogenoantimonates(III) crystals.

V. CONCLUSIONS

(i) $[4\text{-}NH_2C_5H_4NH][SbCl_4]$ appears to be a ferroelectric crystal between 270.5 and 240 K with spontaneous polarization of the order of 3.5 mC/m^2.

(ii) The structure of $[4\text{-}NH_2C_5H_4NH][SbCl_4]$ is characterized by static polyanionic $(SbCl_4{}^-)_n$ units and disordered organic cations (at room temperature).

(iii) From the x-ray data the following mechanism of the phase transitions is proposed. In the paraelectric phase, $C2/c$ (278 K), the 4-aminopyridinium cations are distributed between two positions with occupation factors of 0.5/0.5. All cations (type *A*) reorient in the (201) plane by about 135°. The ferroelectric transition to the *Cc* phase ($T_{c2}=270.5$ K) is related to the setting of this motion so only one position is occupied (cation type *C*).

[1] R. Jakubas and L. Sobczyk, Phase Transitions **20**, 163 (1990).
[2] V. Varma, R. Bhattacharjee, H. N. Vasan, and C. N. R. Rao, Spectrochim. Acta, Part A **48**, 1631 (1992).
[3] L. Sobczyk, R. Jakubas, and J. Zaleski, Pol. J. Chem. **71**, 265 (1997) (and references cited therein).
[4] H. Ishihara, K. Yamada, T. Okuda, and A. Weiss, Bull. Chem. Soc. Jpn. **66**, 380 (1993).
[5] A. Kallel and J. W. Bats, Acta Crystallogr., Sect. C: Cryst. Struct. Commun. **C41**, 1022 (1985).
[6] B. Chabot and E. Parthe, Acta Crystallogr., Sect. B: Struct. Crystallogr. Cryst. Chem. **B34**, 645 (1978).
[7] R. Jakubas, U. Krzewska, G. Bator, and L. Sobczyk, Ferroelectrics **77**, 129 (1988).
[8] J. Zaleski and A. Pietraszko, Acta Crystallogr., Sect. B: Struct. Sci. **B52**, 287 (1996).
[9] M. Bujak and J. Zaleski, Cryst. Eng. **4**, 241 (2001).
[10] G. Bator, R. Jakubas, J. Zaleski, and J. Mróz, J. Appl. Phys. **88**, 1015 (2000).
[11] R. Jakubas, Solid State Commun. **69**, 267 (1989).
[12] J. Lefebvre, P. Carpentier, and R. Jakubas, Acta Crystallogr. **B51**, 167 (1995).
[13] J. Jóźków, G. Bator, R. Jakubas, and A. Pietraszko, J. Chem. Phys. **114**, 7239 (2001).
[14] Oxford Diffraction 2001, CrysAlis ''CCD'' and CrysAlis ''RED,'' Oxford Diffraction (Poland) Sp. z.o.o, Wroclaw, Poland.
[15] G. M. Sheldrick, SHELXS97, program for solution of crystal structures (University of Göttingen, Göttingen, 1997).
[16] G. M. Sheldrick, SHELXL97, program for crystal structure refinement (University of Göttingen, Göttingen, 1997).
[17] CCDC No. 185826–185828. Copies of this information may be obtained free of charge from the Director, CCDC, 12 UNION Road, Cambridge CB2 1EZ, UK (fax: +44-1223-336033; e-mail:deposit@ccdc.cam.ac.uk or http://www.ccdc.cam.ac.uk).
[18] E. Fatuzzo and W. J. Merz, *Ferroelectricity* (North-Holland, Amsterdam, 1967), p. 115.
[19] V. K. Wadhawan, *Introduction to Ferroic Materials* (Gordon & Breach, New York, 2000).
[20] V. Dvorak, Ferroelectrics **7**, 1 (1974).
[21] I. S. Zheludev, Pramana **9**, 385 (1977).
[22] B. A. Strukov and A. P. Levanyuk, *Ferroelectric Phenomena in Crystals* (Springer, Berlin, 1998), p. 73.
[23] R. Jakubas and G. Bator (unpublished).
[24] I. Hatta, J. Phys. Soc. Jpn. **24**, 1043 (1968).
[25] Y. Takayama, K. Deguchi, and E. Nakamura, J. Phys. Soc. Jpn. **53**, 4121 (1984).
[26] R. Jakubas, H. A. Kołodziej, and L. Sobczyk, J. Phys. C **12**, L49 (1979).
[27] A. Pietraszko, B. Bednarska-Bolek, R. Jakubas, and P. Zieliński, J. Phys.: Condens. Matter **13**, 6471 (2001) and references cited therein.